Nano Research 2015, 8(7): 2261–2270
DOI 10.1007/s12274-015-0737-7
Research Article
ISSN 1998-0124
CN 11-5974/O4

Hexagonally arranged arrays of urchin-like Ag hemispheres decorated with Ag nanoparticles for surface-enhanced Raman scattering substrates

Haibin Tang[1], Guowen Meng[1,2] (✉), Zhongbo Li[1], Chuhong Zhu[1], Zhulin Huang[1], Zhaoming Wang[1], and Fadi Li[1]

[1] *Key Laboratory of Materials Physics, and Anhui Key Laboratory of Nanomaterials and Nanotechnology, Institute of Solid State Physics, Chinese Academy of Sciences, P. O. Box 1129, Hefei 230031, China*
[2] *University of Science and Technology of China, Hefei 230026, China*

Received: 20 November 2014
Revised: 19 January 2015
Accepted: 23 January 2015

KEYWORDS
Ag-hemisphere,
urchin-like,
surface roughness,
polychlorinated biphenyls (PCBs),
surface-enhanced Raman scattering (SERS)

ABSTRACT

The surface topography of noble metal particles is a significant factor in tailoring surface-enhanced Raman scattering (SERS) properties. Here, we present a simple fabrication route to hexagonally arranged arrays of surface-roughened urchin-like Ag hemispheres (Ag-HSs) decorated with Ag nanoparticles (Ag-NPs) for highly active and reproducible SERS substrates. The urchin-like Ag-HS arrays are achieved by sputtering Ag onto the top surface of a highly ordered porous anodic aluminum oxide (AAO) template to form ordered arrays of smooth Ag-HSs and then by electrodepositing Ag-NPs onto the surface of each Ag-HS. Owing to the ordered arrangement of the Ag-HSs and the improved surface roughness, the urchin-like hierarchical Ag-HS arrays can provide sufficient and uniform "hot spots" for reproducible and highly active SERS effects. Using the urchin-like Ag-HS arrays as SERS substrates, 10^{-7} M dibutyl phthalate (a member of plasticizers family) and 1.5×10^{-5} M PCB-77 (one congener of polychlorinated biphenyl, a notorious class of pollutants) are identified, showing promising potential for these substrates in the rapid recognition of organic pollutants.

1 Introduction

Surface-enhanced Raman scattering spectroscopy (SERS) has drawn much attention in biological, chemical, and environmental fields for its high sensitivity, fast response, and fingerprint identification [1–4]. From the perspective of the electromagnetic enhancement mechanism, the SERS effect is highly dependent on the nanoparticle (NP) size and shape as it relates to the excitation wavelength and dielectric properties of the medium [5, 6]. Additionally, the surface topography of the particles can also be a significant factor in tailoring the optical properties. Surface roughness of only a few atomic layers can generate red shifts of longitudinal surface plasmon modes [7, 8]. As a result, the SERS performance of

Address correspondence to gwmeng@issp.ac.cn

noble metal mesoscopic particles with irregular nanoscale surface roughness or with deeply creviced surface morphology has attracted increasing research interest [9–12]. For example, Halas et al. synthesized Au "meatball-like" particles with randomly arranged irregular nanoscale protrusions through an organic reduction using gum Arabic as the stabilizer [10]. Xu et al. prepared highly surface-roughened "flower-like" Ag-NPs with polyvinyl pyrrolidone (PVP) surfactant in an aqueous environment [11]. Fang et al. synthesized urchin-like Au mesoparticles with a tailored surface topography via secondary nucleation and growth method or oil/water interface synthesis method; the resulting spike-covered urchin-like mesoparticles exhibit high SERS sensitivity [5, 6]. Yang et al. synthesized star-like Ag nanocrystals via a highly anisotropic etching process using NH_4OH/H_2O_2 as the etchant and PVP as the stabilizing agent [13]. The rough surface of these hierarchical noble metal particles could induce higher SERS activity. Nevertheless, most of these plasmonic nanostructures are obtained through organic reduction routes using specific stabilizers or surfactants in solution, which might introduce signal interference in the subsequent SERS measurement. In addition to the high SERS activity, signal uniformity is another important issue for SERS substrates in practical applications. However, it is still a challenge to uniformly disperse hierarchical particles synthesized in solution on planar substrates to achieve a uniform and reproducible SERS signal response. In our previous work, we fabricated urchin-like Ag nanohemisphere arrays decorated with Au-NPs by sputtering Au-NPs (~10 nm) onto the Ag nanohemispheres (~90 nm), which had been molded by nanopores of oxalic acid-oxidized anodic aluminum oxide (AAO) templates [14]. Using the sputtering method, only small heteromaterials (such as Au) could be applied to the surface of the Ag nanohemispheres; however, an Ag nanostructure with higher SERS activity could not be applied onto the surface. Moreover, the surface roughness was low for the small size of the Au-NPs.

Herein, we present a rational route to electrochemically assemble homogeneous Ag-NPs with a larger size (30–50 nm) onto the surface of Ag hemisphere (Ag-HS) arrays molded by pores of phosphoric-acid-derived AAO template, achieving two-dimensional (2D) hexagonally arranged urchin-like Ag-HS arrays with higher surface roughness, as shown schematically in Scheme 1. First, Ag is sputtered onto the top surface of the highly ordered and hexagonally arranged porous AAO template, and Ag aggregations occur and expand downwards in the AAO pores to form Ag-HSs within the pores [15]. With continued Ag sputtering, the pores are blocked and Ag film is created on the top surface of AAO. Then, hot-melt adhesives are spread on the top surface of the Ag film to fix and support the Ag-HSs array. After removing the AAO template, the 2D uniform hexagonally arranged Ag-HS (with smooth surface) arrays are supported on the hot-melt adhesive film. Finally, small Ag-NPs are electrodeposited onto each Ag-HS surface using a low current density to achieve 2D hexagonally ordered urchin-like Ag-HS arrays. The resultant urchin-like Ag-HS arrays show reproducible and high SERS activity to rhodamine 6G (R6G). As a trial for practical applications, the urchin-like Ag-HS arrays have been used for SERS-based recognition of dibutyl phthalate (DBP, a frequently used plasticizer [16–18] that is harmful to human health) and polychlorinated biphenyls (PCBs, one class of persistent organic pollutants (POPs) defined by the Stockholm Convention [19–22]). A low detection concentration of 10^{-7} M for DBP and 1.5×10^{-5} M for PCB-77 (one congener of PCBs) has been identified. Therefore, the urchin-like Ag-HS arrays have potential for the SERS-based rapid recognition of

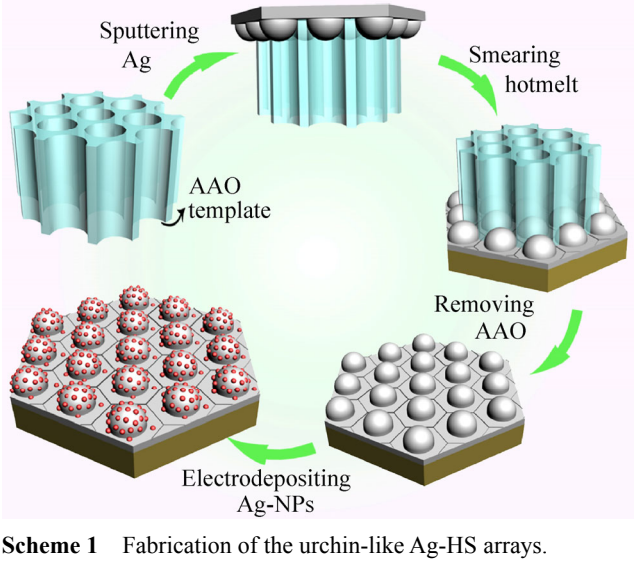

Scheme 1 Fabrication of the urchin-like Ag-HS arrays.

organic pollutants such as plasticizers and PCBs in the environment.

2 Experimental

2.1 Fabrication of the urchin-like Ag-HS arrays

The AAO templates with highly ordered and hexagonally arranged nanopores were prepared via a two-step anodization of Al foil in 0.3 M phosphoric acid under DC of 195 V at –5 ℃ [23]. The pores were etched through and widened in 5% (wt.) phosphoric acid at 45 ℃ for 40 min. To produce Ag-HSs within the pores, Ag was sputtered onto the top surface of the phosphoric-acid-derived AAO template using an ion sputter (EDT-3000) for 30 min with a current of 5 mA and vacuum of 1.2×10^{-1} mBar [14]. Then, hot-melt adhesive was spread on the top surface of the Ag film to fix and support the Ag-HS arrays. Next, the AAO template was removed in 1 M NaOH solution for 30 min, achieving 2D hexagonally arranged uniform Ag-HS arrays supported on the hot-melt adhesive film. Finally, small Ag-NPs were electrochemically deposited onto the Ag-HSs surface using an electrolyte of 20 mM $AgNO_3$ and 10 mM citric acid with a graphite sheet as anode, resulting in 2D uniformly arranged urchin-like Ag-HS arrays.

2.2 Characterization

The as-prepared arrays were characterized using scanning electron microscopy (SEM, SIRION 200, HITACHI SU8020). The SERS spectra were recorded by a confocal Raman system (Renishaw, inVia). The excitation wavelength of 532 nm was generated by an air-cooled argon ion laser. The laser power was 0.1 mW in the SERS measurement for R6G and DBP and 5 mW for PCB-77 detection. In the SERS characterization, the as-prepared substrates were firstly modestly sputtered for 3 min in plasma cleaner (PDC-32G) to remove the citric acid on the surface, and then immersed in R6G or DBP solution with different concentrations for 4 h. Note that the modest plasma cleaning will not damage the morphology of the Ag-nanostructures. However, high intensity and long duration (10 min) plasma cleaning would change or destroy the as-prepared structures, as shown in Fig. S1 in the Electronic Supplementary Material (ESM). For identifying PCB-77, 2 μL of PCB-77 acetone solutions from 10^{-4} to 5×10^{-6} M were dropped onto the as-prepared substrates. This procedure was repeated three times to ensure uniform SERS signal.

3 Results and discussion

3.1 Morphology and structure

As shown in Figs. 1(a) and 1(b), owing to the successful replication of the ordered AAO-pores, large-scale hexagonally arranged Ag-HSs with smooth surface are achieved. The average diameter of the Ag-HSs is about 195 nm with a neighboring center-to-center separation of 370 nm. Between any two neighboring hexagonal cells, there exists a gap of about 15 nm, which is an exact copy of the protuberance around the cell boundary that is caused by the etching rate difference between the pore inner wall and outer wall in phosphoric acid solution [23–25]. These 15-nm gaps also contribute to the SERS activity in the "hot spot." After assembling Ag-NPs onto the surface via electrodeposition at 8 μA/mm^2 for 30 s in 20 mM $AgNO_3$ and 10 mM citric acid electrolyte, urchin-like Ag-HSs have been achieved, as shown in Figs. 1(c) and 1(d).

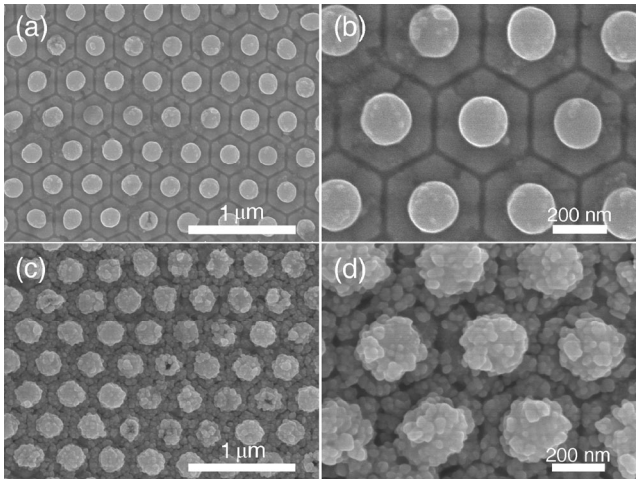

Figure 1 (a) The SEM image and (b) enlarged image of the large-scaled and hexagonally arranged Ag-HS array with a smooth surface; (c) the SEM image and (d) enlarged image of the urchin-like hexagonally arranged Ag-HS array.

The 30–50-nm-diameter Ag-NPs were coated on the whole surface of the Ag-HSs, and the surface roughness of the Ag-HS is obviously improved. Meanwhile, the gaps between the neighboring cells narrow to 10 nm or less after the Ag-NPs are assembled, which will also contribute to the improved SERS activity.

3.2 Influence of current density and citric acid

The morphological development of the urchin-like Ag-HS arrays with different current densities and citric acid concentrations is revealed in Figs. 2 and 3, respectively. Citric acid is usually used as a capping agent for strong binding to {111} facets in the electrodeposition of Ag nanosheets [26, 27]. Here, Ag-NPs have been electrodeposited on the surface of the Ag-HS arrays with citric acid as the capping agent. At the current density of 1 μA/mm^2, small Ag-NPs with diameters of 10 nm are assembled onto the surface of each Ag-HS, as shown in Fig. 2(a). With the increase of the current density to 5 μA/mm^2, Ag-NPs with larger diameter (50–80 nm) are achieved on the surface of each Ag-HS, creating an urchin-like morphology, as shown in Fig. 2(b). After optimizing the electrodeposition at a current density of 8 μA/mm^2 for 30 s, a large number of Ag-NPs are assembled over the whole surface of each Ag-HS, as shown in Figs. 1(c) and 1(d). If the current density is further increased to 16 μA/mm^2, Ag nanosheets with a width of 100 nm are deposited onto the surface of each Ag-HS instead of NPs, leading to flower-like Ag particle arrays, as shown in Fig. 2(c). At a much higher current density (30 μA/mm^2), the reduction rate will be fast, and Ag dendrites are generated on the surface of the Ag-HS array substrate but not on the surface of each Ag-HS, as shown in Fig. 2(d).

On the other hand, citric acid also has a significant impact on the development of the Ag-NPs. As shown in Fig. 3(a), without citric acid in the electrolyte, small Ag-NPs cannot be generated on the surface of each Ag-HS, but randomly distributed micron-sized Ag-particles are produced on the substrate surface. When a low concentration of citric acid (1 mM) is added into the electrolyte, 20-nm spherical Ag structures can be deposited onto the surface of the Ag-HSs, as shown in Fig. 3(b). With an increase in the citric acid concentration from 1 to 25 mM, the spherical Ag-NPs become more distinct and separated with a gradual increase in size, as shown in Figs. 3(b)–3(d). With Ag-NP growth, the gaps between neighboring hexagonal cells become narrower. If the concentration

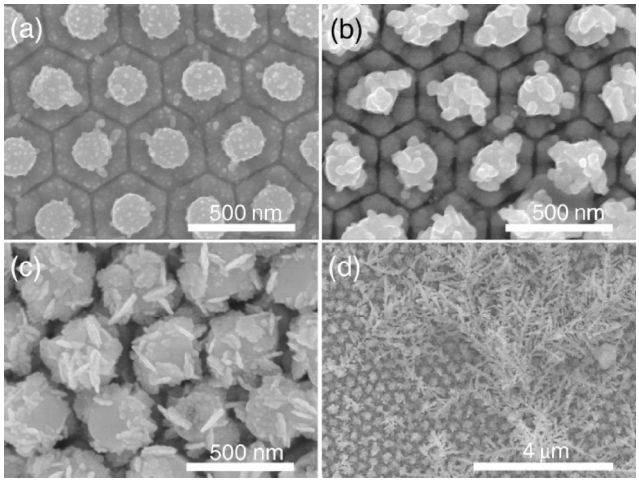

Figure 2 The SEM images of the as-prepared urchin-like Ag-HS arrays fabricated at different current densities for 60 s in an electrolyte of 20 mM $AgNO_3$ and 10 mM citric acid: (a) 1, (b) 5, (c) 16, and (d) 30 μA/mm^2.

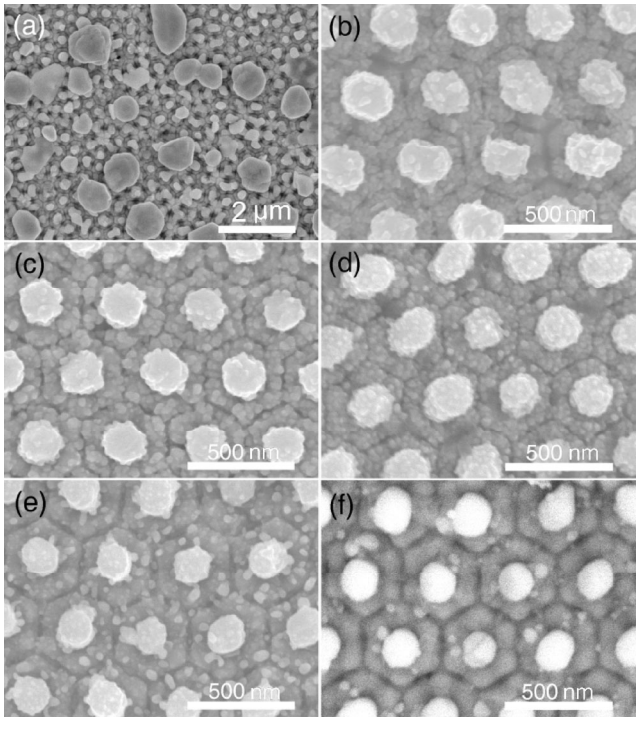

Figure 3 The SEM images of the as-prepared urchin-like Ag-HS arrays fabricated with different concentrations of citric acid for 40 s with 20 mM $AgNO_3$ at a current density of 5 μA/mm^2: (a) 0, (b) 1, (c) 10, (d) 25, (e) 50, and (f) 100 mM.

of citric acid is further increased, the size of the Ag-NPs obviously increases; however, the number of Ag-NPs coated on the Ag-HS surface decreases, as shown in Figs. 3(e) and 3(f) for citric acid concentrations of 50 and 100 mM, respectively.

The Ag-NP growth mechanism now becomes clear. With citric acid as the dispersing agent, the number of nucleation centers is increased. The Ag ions are slowly reduced to Ag, which then grow into Ag-NPs on the substrate surface and especially on the surface of each Ag-HS at low current density (1–10 μA/mm^2). With increasing citric acid concentration, more citrate is adsorbed on the Ag-HS array substrate, reducing the number of nucleation sites for the electrical reduction of Ag ions to Ag-NPs. Consequently, the number of the Ag-NPs decreases and the size of the Ag-NPs increases with the increase in citric acid concentration. At moderate current density (15–25 μA/mm^2), the reduction rate of the Ag ions obviously increases; meanwhile, with citric acid as the capping agent, Ag nanosheets are achieved at a high growth rate on the facets parallel to {111} [26, 27]. At high current density (30 μA/mm^2), the reduction rate is extremely high, and Ag dendrites are directly generated on the substrate surface.

3.3 Influence of electrodeposition duration

The morphological evolution of Ag-HS arrays with the electrodeposition duration at different current densities is shown in Fig. 4 and Fig. S2 in the ESM. With prolonged electrodeposition, both the number and size of the Ag-NPs increase for two different current densities of 1 (Fig. 4) and 8 μA/mm^2 (Fig. S2 in the ESM). With a low current density (1 μA/mm^2), the production of Ag-NPs is slow. For short electrodeposition duration (15 s), only irregularly shaped Ag clusters are assembled onto the surface of the Ag-HSs and the hexagonal cells. As the electrodeposition duration is increased, the number and size of the Ag-NPs gradually increase, as shown in Figs. 4(b) and 4(c) for electrodeposition durations of 30 and 60 s. When the electrodeposition duration is extended to 90 s, the surface of the Ag-HSs and hexagonal Ag cells is uniformly coated with spherical Ag-NPs with diameters of 20–30 nm, as shown in Fig. 4(d). The increase in the number and size of Ag-NPs continues for the electrodeposition duration of 120 s, as shown in Fig. 4(e). Once the electrodeposition is prolonged to 180 s, island-like Ag-NPs with larger dimensions (40–70 nm) are assembled on the surface of the Ag-HSs, while the spacing between the neighboring Ag-HSs obviously decreases. On the other hand, with a high current density (8 μA/mm^2), the production of Ag-NPs is obviously increased, as shown in Fig. S2(a) in the ESM. For the short electrodeposition duration of 15 s, Ag clusters are still coated on the surface of the Ag-HSs and the hexagonal Ag cells. However, after electrodeposition for 30 s, a large number of Ag-NPs with a dimension of 50 nm were assembled on the whole surface of the Ag-HSs and the hexagonal Ag cells, and the total diameter of the urchin-like Ag-HS is increased to 230 nm, as shown in Fig. S2(b) in the ESM. When the electrodeposition duration is prolonged to 45 s, 50-nm Ag-NPs and clusters of Ag-NPs with a dimension of 100–150 nm are coated on the surface of the Ag-HSs, and the resultant total diameter of the urchin-like Ag-HSs reaches ~300 nm, as shown in Fig. S2(c) in the ESM.

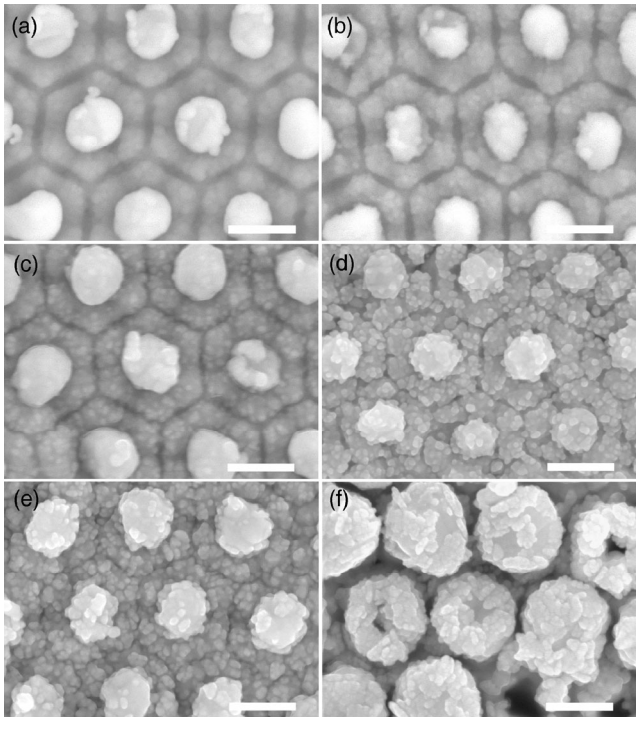

Figure 4 The SEM images of the as-prepared urchin-like Ag-HS arrays fabricated for different electrodeposition durations at a current density of 1 μA/mm^2: (a) 15, (b) 30, (c) 60, (d) 90, (e) 120, and (f) 180 s. Scale bar: 250 nm.

3.4 The SERS performance and applications

Using 1 × 10^{-8}-M R6G as the probe molecule, the SERS performance of the hexagonally arranged urchin-like Ag-HS arrays is shown in Fig. 5. Figure 5(a) reveals that, after the electrodeposition of Ag-NPs (with the current density of 1 to 8 μA/mm^2) onto the surface of the Ag-HS, the SERS-activity is improved. The urchin-like Ag-HS array achieved at a current density of 8 μA/mm^2 has the optimal SERS sensitivity. The improved SERS activity of the urchin-like Ag-HS arrays can be ascribed to the decoration of the Ag-NPs with improved roughness [5, 6, 8], and to the improved density of optical modes for the long-rang periodic structure [28–30] as well as the electromagnetic coupling at the gaps between neighboring Ag-NPs and the gaps between neighboring hexagonal cells, as shown in Fig. 1(d). On the other hand, the SERS activity of the urchin-like Ag-HS array under a current density of 5 μA/mm^2 decreases slightly. This phenomenon could be induced by the inequitable morphology of the Ag-NPs located on the Ag-HS surface. As shown in Fig. 2(b), there are fewer gaps between the Ag-NPs, i.e., fewer SERS hot spots, compared with substrates fabricated with current density of 1 or 8 μA/mm^2. For the same reason, the SERS activity of the substrates fabricated with higher current densities (16 and 30 μA/mm^2) sharply decreases. Additionally, the SERS sensitivity dependence of substrates fabricated with current densities of 1 and 8 μA/mm^2 on the electrodeposition duration is revealed in Fig. 5(b) and Fig. S3 in the ESM. The SERS activity of the substrate electrodeposited for 30 s is improved over that for 15 s and maintains a similar activity level as the electrodeposition duration is further increased. At an electrodeposition time of 180 s, the SERS activity sharply decreases. This evolution law can be understood by illustrating the character of the morphology shown in Fig. 4. After a short electrodeposition (15 s), as shown in Fig. 4(a), only a few Ag-NPs are created on the Ag-HS surface; with elongated electrodeposition, the number of both the Ag-NPs and neighboring gaps (SERS hot spots) increases, consequently improving the SERS activity. As the electrodeposition duration increases from 30 to 120 s, the size of the Ag-NPs gradually increases,

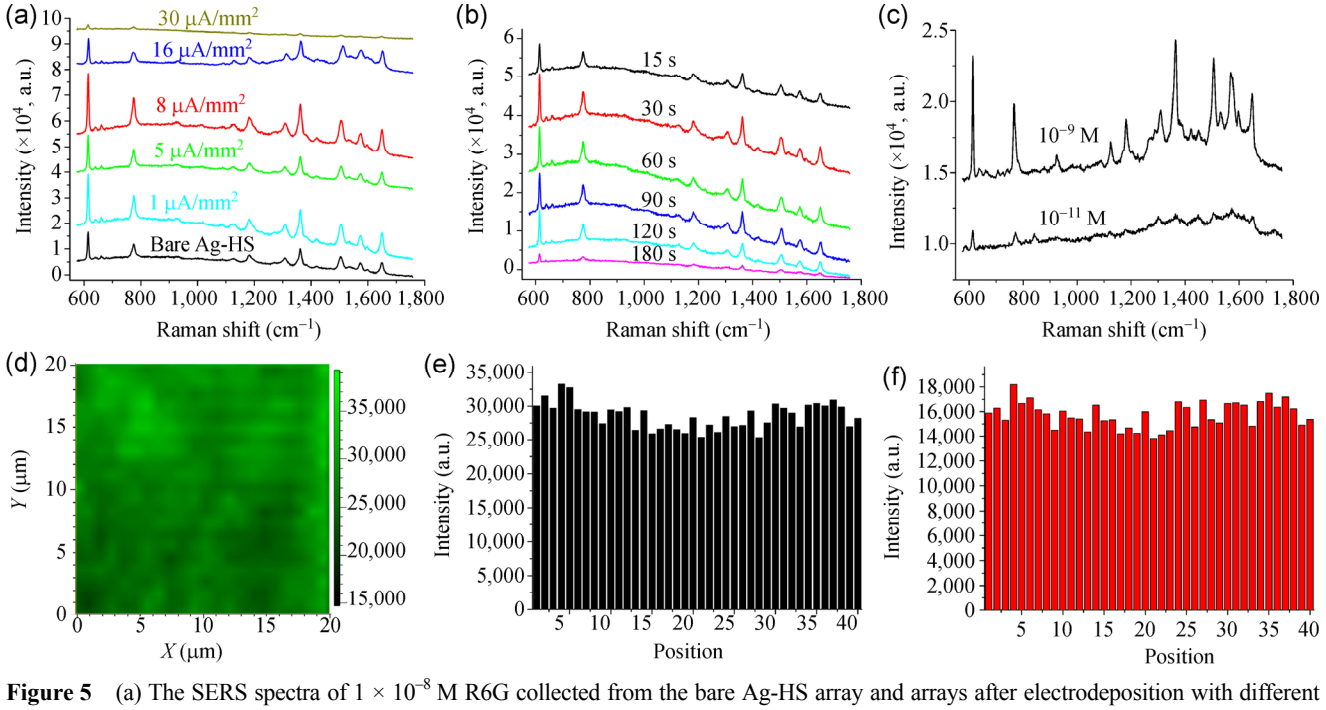

Figure 5 (a) The SERS spectra of 1 × 10^{-8} M R6G collected from the bare Ag-HS array and arrays after electrodeposition with different current densities. (b) The SERS sensitivity of the urchin-like Ag-HS array with different electrodeposition durations at a current density of 1 μA/mm^2. (c) The SERS sensitivity of the optimal substrates to low concentration R6G with an integration time of 10 s. (d) The SERS mapping of 1,362 cm^{-1} and intensity statistics of the characteristic peaks at (e) 614 and (f) 1,362 cm^{-1} collected from 40 random spots on the as-prepared urchin-like Ag-HS array substrate.

but the neighboring gaps do not undergo dramatic changes, as shown in Figs. 4(b)–4(e); thus, the SERS activity is unchanged. For excessively long electrodeposition (180 s), the gaps decrease due to the aggregation of Ag-NPs, and the SERS activity sharply decreases. The same phenomenon is also observed for substrates electrodeposited at 8 μA/mm^2, as shown in Fig. S3 in the ESM.

The SERS activity of the urchin-like Ag-HS arrays is tested using R6G (with different concentrations of 1×10^{-9} and 1×10^{-11} M) as the probe molecules. As shown in Fig. 5(c), low concentration R6G (1×10^{-11} M) can be still easily distinguished, and the main characteristic peaks of R6G at 614, 775, and 1,362 cm^{-1} are assigned to the C–C–C ring in-plane bending mode, C–H out of plane bending mode, and aromatic C–C stretching vibration mode, respectively [31, 32]. The high SERS activity is also revealed by the enhancement factor (EF) estimation, shown in detail in Part S4 in the ESM, where 4-aminothiophenol (4-ATP) probe molecules were used for more precise estimation of the absorbed molecules that contribute to the SERS signal intensity. The average EF is estimated to be 1.23×10^6, confirming high SERS activity of the resultant hexagonally arranged urchin-like Ag-HS arrays.

The signal uniformity of the urchin-like Ag-HS arrays, which is one of the other important factors for practical SERS substrates, is also manifested using 1×10^{-7} M R6G as the probe molecules. The SERS mapping of the 1,362 cm^{-1} peak and the spectra collected from 40 random spots on the as-prepared urchin-like Ag-HS array substrate are shown in Fig. 5(d) and Fig. S6 in the ESM, respectively. The uniform signal distribution and the similar intensity of each characteristic peak of the 40 spectra demonstrate good signal uniformity. For a more detailed analysis, the intensity of the characteristic peaks at 614 and 1,362 cm^{-1} of the random 40 spectra is statistically shown in Figs. 5(e) and 5(f), respectively. The relative standard deviation of the intensity of the characteristic peak at 614 and 1,362 cm^{-1} is calculated to be 6.77% and 6.69%, respectively, revealing good signal uniformity of the urchin-like Ag-HS arrays. The reason for the good signal uniformity of the as-prepared substrate can be attributed to the large-scale morphology uniformity of the Ag-HS array self-supported on the hot-melt adhesive film substrate, which is reproduced from the hexagonally ordered pores of the AAO templates, as shown in Fig. 1(a). Additionally, as Ag nanostructures are easily oxidized and sulfured in air, the stability of the as-prepared substrate is tested, as shown in Fig. S7 in the ESM. The SERS activity of the substrates can maintain a relatively high level after two months, while the SERS activity sharply decreases after six months.

Finally, the urchin-like Ag-HS arrays are used as SERS-substrates to detect plasticizer and PCB-77. The plasticizer DBP, as one of the most important members in the phthalate family, has been used in food packaging, children's products, and medical devices. However, exposure to phthalate plasticizers may increase prevalence of asthma, rhinitis, or wheezing [16–18], cause reproductive disorders in humans, and affect endogenous hormones [33, 34]. Using the as-prepared urchin-like Ag-HS arrays as SERS substrates, different concentrations (10^{-4}, 10^{-6}, 10^{-7} M) of DBP were detected, as shown in Fig. 6(a). Even for 10^{-7} M DBP, the characteristic vibration bands of DBP can be identified. Similarly, different concentrations (3×10^{-4}, 1.5×10^{-4}, 3×10^{-5}, 1.5×10^{-5} M) of PCB-77 have been detected, as shown in Fig. 6(b). The characteristic vibration bands of PCB-77 with a low concentration (1.5×10^{-5} M) can be identified and assigned as follows: The bands at 676 and 1,136 cm^{-1} belong to the C–Cl stretching mode, the band at 1,297 cm^{-1} is assigned to the C–C bridge stretching mode, and the band at 1,599 cm^{-1} is attributed to the aromatic vibration modes [35–37].

4 Conclusions

In summary, uniform 2D monolayer-dispersed and hexagonally arranged urchin-like Ag-HS arrays have been fabricated via an AAO template-assisted approach and show excellent SERS performance. The Ag-HSs are formed at the ordered pores of the AAO template and replicate the large-scale ordered pattern of the AAO-pores, resulting in large-scale hexagonally arranged Ag-HSs. Furthermore, a large number of small Ag-NPs are decorated onto the surface of the

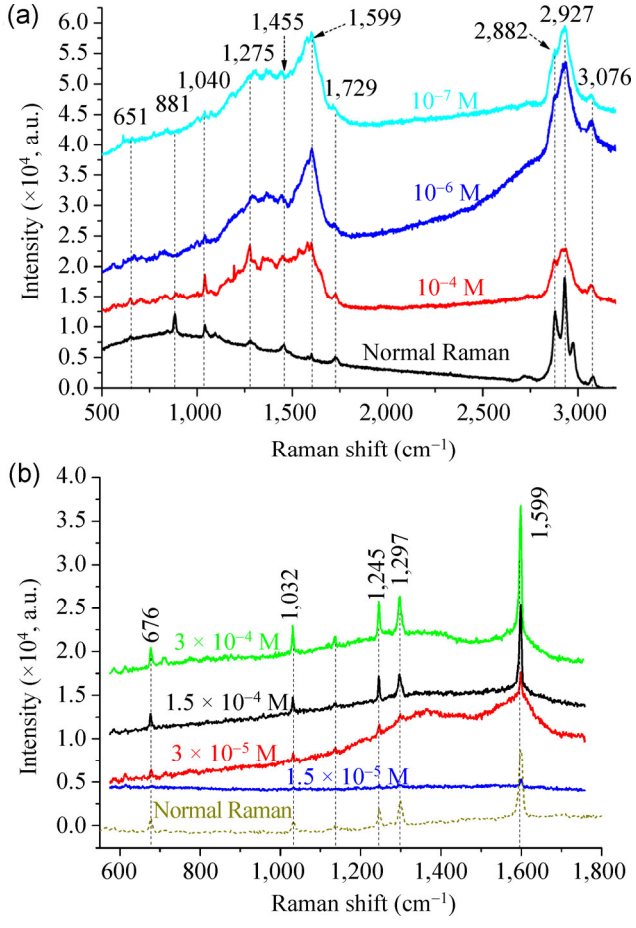

Figure 6 The SERS spectra of (a) DBP and (b) PCB-77 with different concentrations collected using the as-prepared urchin-like Ag-HS arrays. The corresponding normal Raman spectra are shown in the bottom of each pattern.

Ag-HSs via electrodeposition, forming urchin-like Ag-HS arrays. Thus, the SERS sensitivity is further improved owing to the enhanced surface-roughness and electromagnetic coupling. The resultant substrates demonstrate high SERS sensitivity to 10^{-11} M R6G, 10^{-7} M DBP, and 1.5×10^{-5} M PCB-77. Therefore, the hexagonally arranged urchin-like Ag-HS arrays have great potential as effective SERS substrates for rapid detection and monitoring of trace organic pollutants.

Acknowledgements

This work was financially supported by the National Basic Research Program of China (No. 2013CB934304), the CAS/SAFEA International Partnership Program for Creative Research Teams, the National Natural Science Foundation of China (Nos. 21303211, 11274312 and 51472245).

Electronic Supplementary Material: Supplementary material (SEM images and SERS activity of the urchin-like Ag-HS arrays fabricated at different electrodeposition durations; estimation of the enhanced factor and the signal uniformity) is available in the online version of this article at http://dx.doi.org/10.1007/s12274-015-0736-8.

References

[1] Ling, X. Y.; Yan, R. X.; Lo, S.; Hoang, D. T.; Liu, C.; Fardy, M. A.; Khan, S. B.; Asiri, A. M.; Bawaked, S. M.; Yang, P. D. Alumina-coated Ag nanocrystal monolayers as surface-enhanced Raman spectroscopy platforms for the direct spectroscopic detection of water splitting reaction intermediates. *Nano Res.* **2014**, *7*, 132–143.

[2] Schlücker, S. Surface-enhanced Raman spectroscopy: Concepts and chemical applications. *Angew. Chem. Int. Ed.* **2014**, *53*, 4756–4795.

[3] Nima, Z. A.; Mahmood, M.; Xu, Y.; Mustafa, T.; Watanabe, F.; Nedosekin, D. A.; Juratli, M. A.; Fahmi, T.; Galanzha, E. I. et al. Circulating tumor cell identification by functionalized silver-gold nanorods with multicolor, super-enhanced SERS and photothermal resonances. *Sci. Rep.* **2014**, *4*, 4752.

[4] Huang, Z. L.; Meng, G. W.; Huang, Q.; Chen, B.; Zhou, F.; Hu, X. Y.; Qian, Y. W.; Tang, H. B.; Han, F. M.; Chu, Z. Q. Polyacrylic acid sodium salt film entrapped Ag-nanocubes as molecule traps for SERS detection. *Nano Res.* **2014**, *7*, 1177–1187.

[5] You, H. J.; Ji, Y. T.; Wang, L.; Yang, S. C.; Yang, Z. M.; Fang, J. X.; Song, X. P.; Ding, B. J. Interface synthesis of gold mesocrystals with highly roughened surfaces for surface-enhanced Raman spectroscopy. *J. Mater. Chem.* **2012**, *22*, 1998–2006.

[6] Fang, J. X.; Du, S. Y.; Lebedkin, S.; Li, Z. Y.; Kruk, R.; Kappes, M.; Hahn, H. Gold mesostructures with tailored surface topography and their self-assembly arrays for surface-enhanced Raman spectroscopy. *Nano Lett.* **2010**, *10*, 5006–5013.

[7] Pechárroman, C.; Pérez-Juste, J.; Mata-Osoro, G.; Liz-Marzán, L. M.; Mulvaney, P. Redshift of surface plasmon modes of small gold rods due to their atomic roughness and end-cap geometry. *Phys. Rev. B* **2008**, *77*, 035418.

[8] Rodríguez-Fernández, J.; Funston, A. M.; Perez-Juste, J.;

álvarez-Puebla, R. A.; Liz-Marzán, L. M.; Mulvaney, P. The effect of surface roughness on the plasmonic response of individual sub-micron gold spheres. *Phys. Chem. Chem. Phys.* **2009**, *11*, 5909–5914.

[9] Bakr, O. M.; Wunsch, B. H.; Stellacci, F. High-yield synthesis of multi-branched urchin-like gold nanoparticles. *Chem. Mater.* **2006**, *18*, 3297–3301.

[10] Wang, H.; Halas, N. J. Mesoscopic Au "meatball" particles. *Adv. Mater.* **2008**, *20*, 820–825.

[11] Liang, H. Y.; Li, Z. P.; Wang, W. Z.; Wu, Y. S.; Xu, H. X. Highly surface-roughened "flower-like" silver nanoparticles for extremely sensitive substrates of surface-enhanced Raman scattering. *Adv. Mater.* **2009**, *21*, 4614–4618.

[12] Huang, P.; Pandoli, O.; Wang, X. S.; Wang, Z.; Li, Z. M.; Zhang, C. L.; Chen, F.; Lin, J.; Cui, D. X.; Chen, X. Y. Chiral guanosine 5'-monophosphate-capped gold nanoflowers: Controllable synthesis, characterization, surface-enhanced Raman scattering activity, cellular imaging and photothermal therapy. *Nano Res.* **2012**, *5*, 630–639.

[13] Mulvihill, M. J.; Ling, X. Y.; Henzie, J.; Yang, P. Anisotropic etching of silver nanoparticles for plasmonic structures capable of single-particle SERS. *J. Am. Chem. Soc.* **2010**, *132*, 268–274.

[14] Tang, H. B.; Meng, G. W.; Huang, Q.; Zhu, C. H.; Huang, Z. L.; Li, Z. B.; Zhang, Z.; Zhang, Y. Urchin-like Au-nanoparticles@Ag-nanohemisphere arrays as active SERS-substrates for recognition of PCBs. *RSC Adv.* **2014**, *4*, 19654–19657.

[15] Wang, J.; Huang, L. Q.; Yuan, L.; Zhao, L. H.; Feng, X. H.; Zhang, W. W.; Zhai, L. P.; Zhu, J. Silver nanostructure arrays abundant in sub-5nm gaps as highly Raman-enhancing substrates. *Appl. Surf. Sci.* **2012**, *258*, 3519–3523.

[16] Jaakkola, J. J. K.; Ieromnimon, A.; Jaakkola, M. S. Interior surface materials and asthma in adults: A population-based incident case-control study. *Am. J. Epidemiol.* **2006**, *164,* 742–749.

[17] Yanagisawa, R.; Takano, H.; Inoue, K. I.; Koike, E.; Sadakane, K.; Ichinose, T. Effects of maternal exposure to di-(2-ethylhexyl) phthalate during fetal and/or neonatal periods on atopic dermatitis in male offspring. *Environ. Health Persp.* **2008**, *116*, 1136–1141.

[18] Kolarik, B.; Naydenov, K.; Larsson, M.; Bornehag, C. G.; Sundell, J. The association between phthalates in dust and allergic diseases among bulgarian children. *Environ. Health Persp.* **2008**, *116*, 98–103.

[19] Zheng, T. Z.; Holford, T. R.; Tessari, J.; Mayne, S. T.; Owens, P. H.; Ward, B.; Carter, D.; Boyle, P.; Dubrow, R.; Archibeque-Engle, S. et al. Breast cancer risk associated with congeners of polychlorinated biphenyls. *Am. J. Epidemiol.* **2000**, *152*, 50–58.

[20] Rylander, L.; Strömberg, U.; Dyremark, E.; Östman, C.; Nilsson-Ehle, P.; Hagmar, L. Polychlorinated biphenyls in blood plasma among swedish female fish consumers in relation to low birth weight. *Am. J. Epidemiol.* **1998**, *147*, 493–502.

[21] Daniels, J. L.; Longnecker, M. P.; Klebanoff, M. A.; Gray, K. A.; Brock, J. W.; Zhou, H. B.; Chen, Z.; Needham, L. L. Prenatal exposure to low-level polychlorinated biphenyls in relation to mental and motor development at 8 months. *Am. J. Epidemiol.* **2003**, *157*, 485–492.

[22] Zhou, Q.; Yang, Y.; Ni, J. E.; Li, Z. C.; Zhang, Z. J. Rapid recognition of isomers of monochlorobiphenyls at trace levels by surface-enhanced Raman scattering using Ag nanorods as a substrate. *Nano Res.* **2010**, *3,* 423–428.

[23] Li, Y. B.; Zheng, M. J.; Ma, L.; Shen, W. Z. Fabrication of highly ordered nanoporous alumina films by stable high-field anodization. *Nanotechnology* **2006**, *17*, 5101.

[24] Choi, J.; Luo, Y.; Wehrspohn, R. B.; Hillebrand, R.; Schilling, J.; Gösele, U. Perfect two-dimensional porous alumina photonic crystals with duplex oxide layers. *J. Appl. Phys.* **2003**, *94*, 4757–4762.

[25] Nielsch, K.; Choi, J.; Schwirn, K.; Wehrspohn, R. B.; Gösele, U. Self-ordering regimes of porous alumina: The 10 porosity rule. *Nano Lett.* **2002**, *2*, 677–680.

[26] Li, Z. B.; Meng, G. W.; Huang, Q.; Zhu, C. H.; Zhang, Z.; Li, X. D. Galvanic-cell-induced growth of Ag nanosheet-assembled structures as sensitive and reproducible SERS substrates. *Chem.—Eur. J.* **2012**, *18*, 14948–14953.

[27] Qian, Y. W.; Meng, G. W.; Huang, Q.; Zhu, C. H.; Huang, Z. L.; Sun, K. X.; Chen, B. Flexible membranes of Ag-nanosheet grafted polyamide-nanofibers as effective 3D SERS substrates. *Nanoscale* **2014**, *6*, 4781–4788.

[28] Duan, G. T.; Cai, W. P.; Luo, Y. Y.; Li, Y.; Lei, Y. Hierarchical surface rough ordered Au particle arrays and their surface enhanced Raman scattering. *Appl. Phys. Lett.* **2006**, *89,* 181918.

[29] Zhang, X.; Zhou, Q.; Wang, W. P.; Shen, L.; Li, Z. C.; Zhang, Z. J. Latticing vertically aligned Ag nanorods to enhance its SERS sensitivity. *Mater. Res. Bull.* **2012**, *47*, 921–924.

[30] Zhang, X.; Zhou, Q.; Ni, J.; Li, Z. C.; Zhang, Z. J. Surface-enhanced Raman scattering from a hexagonal lattice of micro-patterns of vertically aligned Ag nanorods. *Physica E* **2011**, *44*, 460–463.

[31] Cai, Q.; Lu, S. K.; Liao, F.; Li, Y. Q.; Ma, S. Z.; Shao, M. W. Catalytic degradation of dye molecules and *in situ* SERS monitoring by peroxidase-like Au/CuS composite. *Nanoscale* **2014**, *6*, 8117–8123.

[32] Lee, J.; Seo, J.; Kim, D.; Shin, S.; Lee, S.; Mahata, C.; Lee, H. S.; Min, B. W.; Lee, T. Capillary force-induced glue-free printing of Ag nanoparticle arrays for highly sensitive SERS substrates. *ACS Appl. Mater. Inter.* **2014**, *6*, 9053–9060.

[33] Huang, G. L.; Sun, H. W.; Song, Z. H. Interactions between dibutyl phthalate and aquatic organisms. *B. Environ. Contam. Tox.* **1999**, *63*, 759–765.

[34] Mylchreest, E.; Cattley, R. C.; Foster, P. M. D. Male reproductive tract malformations in rats following gestational and lactational exposure to di(n-butyl) phthalate: An antiandrogenic mechanism? *Toxicol. Sci.* **1998**, *43*, 47–60.

[35] Huang, Z. L.; Meng, G. W.; Huang, Q.; Chen, B.; Zhu, C. H.; Zhang, Z. Large-area Ag nanorod array substrates for SERS: AAO template-assisted fabrication, functionalization, and application in detection PCBs. *J. Raman Spectrosc.* **2013**, *44,* 240–246.

[36] Hou, C.; Meng, G. W.; Huang, Q.; Zhu, C. H.; Huang, Z. L.; Chen, B.; Sun, K. X. Ag-nanoparticle-decorated Au-fractal patterns on bowl-like-dimple arrays on Al foil as an effective SERS substrate for the rapid detection of PCBs. *Chem. Commun.* **2014**, *50*, 569–571.

[37] Chen, B.; Meng, G. W.; Huang, Q.; Huang, Z. L.; Xu, Q. L.; Zhu, C. H.; Qian, Y. W.; Ding, Y. Green synthesis of large-scale highly ordered core@shell nanoporous Au@Ag nanorod arrays as sensitive and reproducible 3D SERS substrates. *ACS Appl. Mater. Inter.* **2014**, *6*, 15667–15675.